Homo-tandem-bifacial dye-sensitized solar cell: A new paradigm to boost photoconversion efficiency above limit

(Article begins on next page)
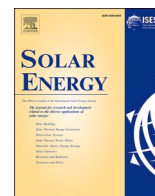
31 December 2024

Homo-tandem-bifacial dye-sensitized solar cell: A new paradigm to boost photoconversion efficiency above limit

Giulia Gianola [a,b], Roberto Speranza [a,b,*], Federico Bella [a], Andrea Lamberti [a,b]

[a] *Politecnico di Torino, Dipartimento di Scienza Applicata e Tecnologia (DISAT), Corso Duca degli Abruzzi, 24, 10129 Turin, Italy*
[b] *Istituto Italiano di Tecnologia, Center for Sustainable Future Technologies, Via Livorno, 60, 10144 Turin, Italy*

ABSTRACT

Over the last three decades, dye-sensitized solar cells (DSSCs) have received a lot of attention, reaching record efficiencies under AM 1.5G illumination slightly over 10%. However, these values are lower than other competing photovoltaic systems. The performance of DSSCs has to be further enhanced in order to have a substantial influence and application potential in the field of photovoltaics. Herein we propose a new intriguing strategy to take advantage of two concepts well known in the field of photovoltaics, such as the tandem configuration and the bifaciality, never applied at the same time to DSSCs. Thanks to the combination of these strategies, we are noteworthy able to overcome the maximum efficiency ever obtained for a traditional DSSC based on iodide/triiodide redox couple and Ru-based dye, as high as 14.96%. Our findings open the way to further enhancement with optimized DSSCs configuration.

1. Introduction

Among different photovoltaic technologies, dye-sensitized solar cells (DSSCs) have always been considered one of the most affordable and cost-effective alternatives to traditional silicon-based solar cells [14,15]. The light harvesting mechanism of DSSCs is based on a dye-sensitized mesoporous film of a wide band gap semiconductor deposited on a transparent conductive substrate to absorb photons and convert them into electrons. A redox mediator in an electrolytic solution closes the circuit with a Pt-coated counter electrode [25]. According to literature, the most commonly employed materials for DSSCs are mainly based on TiO_2 nanoporous electrodes, iodide/triiodide redox couples and Ru-based dyes [4,5,9,36]. Substantial studies have been performed toward the enhancement of DSSCs performances through the engineering of different dyes, electrolytes and electrodes material, with photoconversion efficiencies (PCE) ranging within 11–14% [1,18,21,23].

Apart from materials optimization, different cell configurations have been proposed with the goal of improving the PCE and broadening the application opportunity (e.g., smart buildings, greenhouses, integrated systems with electrocatalytic reactors, *etc.*) [6,16,29] regardless of the employed active materials. In the so-called tandem configuration, multiple dyes are employed in stacked compartments of the cell to maximize the absorbed portion of the light spectrum. In this design, the total active area of the device should remain the same while increasing the amount of light converted into electricity. With this approach, PCE values ranging from 7.5% to 11.3% were reported in the literature [3,34,37,38]. Alternatively, for organic solar cells (OPV), the so-called homo-tandem configuration was also reported, in which a multiple-junction device is fabricated by splitting a single thicker absorbing layer into two half-cells, in order to reduce the travel distance of charge carriers, accounting for their low mobility. Therefore, homo-tandem OPV differs from standard tandem solar cells for the fact that the two absorbing layers are made of the same material [11,12,17,20]. Instead, in bifacial configuration a single compartment solar cell is fabricated in such a way that the device is able to generate photovoltaic power in front and rear illuminations, meaning that it can be illuminated from both the electrodes. In this case, the so-called "bifaciality factor" defines the difference in PCE depending on the illumination direction and is calculated dividing the PCE in rear illumination by the PCE in front illumination [19,26,30,35]. In this work, the combination of these concepts was implemented in the same device, presenting a new configuration called homo-tandem-bifacial dye-sensitized solar cell (HTB-DSSC). In this configuration, the presence of two absorbing layers arranged one behind the other to maximize the absorption of the incoming light was inspired by tandem solar cells. However, opposed to standard tandem solar cells already demonstrated for DSSC, it was

---

decided to have two identical absorbing photoanodes prepared with the same materials, including semitransparent semiconducting oxide and sensitizing dye, similarly to what has been done for homo-tandem OPV. This was done to simplify as much as possible the fabrication of the device, which would be an advantage from the point of view of upscaling the manufacturing process of the proposed configuration. More importantly, it was suggested that the second absorbing layer can improve the overall performance of the device since it would behave as a standard DSSC working under low-light illumination conditions. This is because the intensity of the incoming power reaching the second layer would be reduced as a result of the partial absorption of the first one. It is known that DSSC performances increase under reduced light intensities. Moreover, having two identical semitransparent photoanodes on the two sides would allow to achieve the ability of generating power, with the same performances, both from the front and from the back of the device. This was the feature that was inspired by standard bifacial solar cells. The 3D model of the proposed HTB-DSSC is reported in Fig. 1.

A two-compartment cell was fabricated interposing a bifacial semitransparent shared counter electrode between two identical semitransparent photoanodes. More details about the fabrication of the device and its characterizations are provided in the Appendix. In this configuration, the two half-cells work in parallel with the bottom half-cell that converts into electricity the portion of the incoming light that is not previously absorbed by the top half-cell. Moreover, the two half-cells are fabricated with the same materials, yielding a device that is able to achieve an outstanding bifaciality factor.

2. Results and discussion

When characterized under standard AM 1.5G simulated solar spectrum, the HTB-DSSC showed a PCE of 13.19%, exhibiting a relative improvement in efficiency of 54% with respect to the standard cell, which instead showed a PCE of 8.55% (Table 1). This result sets a first outstanding achievement when compared to the best efficiencies reported for DSSC using N719 dye and I^-/I_3^--based electrolyte, ranging from 9% to values slightly higher than 11% [2,24,27]. From Fig. 2a, it can be seen that the first straightforward reason for this improvement is the higher current density (J_{sc}) photo-generated by the HTB-DSSC with respect to the standard cell, which results from the contribution of the bottom half-cell to the total current. From Table A3, it is clear how the J_{sc} of the HTB-DSSC results to be very close to the sum of the half-cells one. On the other hand, from Fig. 2 it can be seen that the open circuit

Table 1
Summarized photovoltaic parameters under AM 1.5G standard solar spectrum.

Configuration	V_{oc} (V)	J_{sc} (mA cm^{-2})	FF	PCE (%)
Standard DSSC	0.67	18.02	0.70	8.55
HTB-DSSC (front)	0.66	28.11	0.71	13.19
HTB-DSSC (rear)	0.65	28.39	0.69	12.80
HTB-DSSC + mirror	0.68	31.28	0.71	14.96

voltage (V_{oc}) of the HTB-DSSC results to be slightly lower than that of the standard cells. This can be explained by the fact that the bottom half-cell is shielded by the top half-cell and receives a lower amount of incident light. It is known that a reduction in V_{oc} is expected for a decreased light intensity [31]. Therefore, due to the parallel connection between the top and bottom half-cells, the V_{oc} of the HTB-DSSC will result to be in between the two V_{oc} values measured for the standard half-cells. For this reason, precautions to limit the dependence of the V_{oc} from the incident light intensities should be considered in further development of the HTB-DSSC configuration. Nevertheless, thanks to the symmetric nature of the proposed configuration, the PCE could be further improved if a light reflecting mirror is added on the back of the HTB-DSSC. As it can be seen in Fig. 2a, the addition of a back mirror further increases the performance of the solar cell both in terms of J_{sc} and of V_{oc}, yielding to an exceptional PCE of 14.96%.

From these results, the improvements granted by the double absorbing layers within the HTB-DSSC configuration is clear. Nevertheless, to get further insights regarding the extent of the benefits of the proposed design, another experiment was performed, comparing the behavior of the HTB-DSSC configuration with respect to a standard DSSC in which the thickness of the photoanode was doubled. Therefore, a HTB-DSSC was fabricated reducing the thickness of the photoanodes to 6 μm, and it was compared with two standard DSSCs fabricated with photoanode thicknesses of 6 μm and 12 μm. The results of the J-V characterization recorded under AM 1.5G simulated solar spectrum are reported in Fig. A1 and Table A1. This measurement gives a further confirmation of the benefit of having multiple absorbing layers instead of a single, thick photoanode. Indeed, the DSSC with the photoanode thickness of 12 μm shows a higher current with respect to the one with a thinner photoanode (6 μm). On the other hand, a higher effect of the charge carrier recombination is observed both from the reduced open circuit voltage and from the lower shunt resistance observed from the slope of the curve at low voltage values. Instead, the HTB-DSSC still
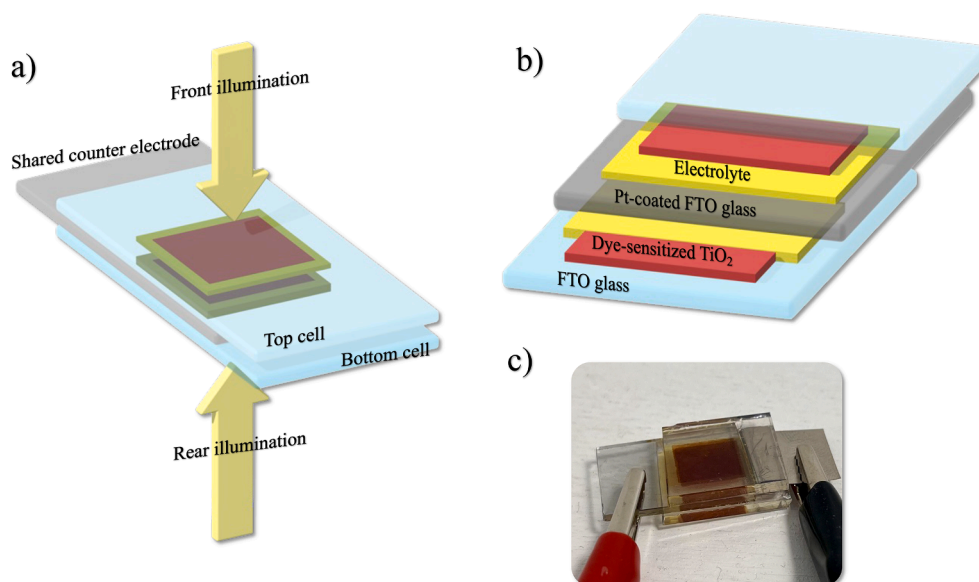
Fig. 1. 3D model (a), section view (b) and photograph of the proposed HTB-DSSC. In panel a) the illumination condition and the half-cell definition are reported.
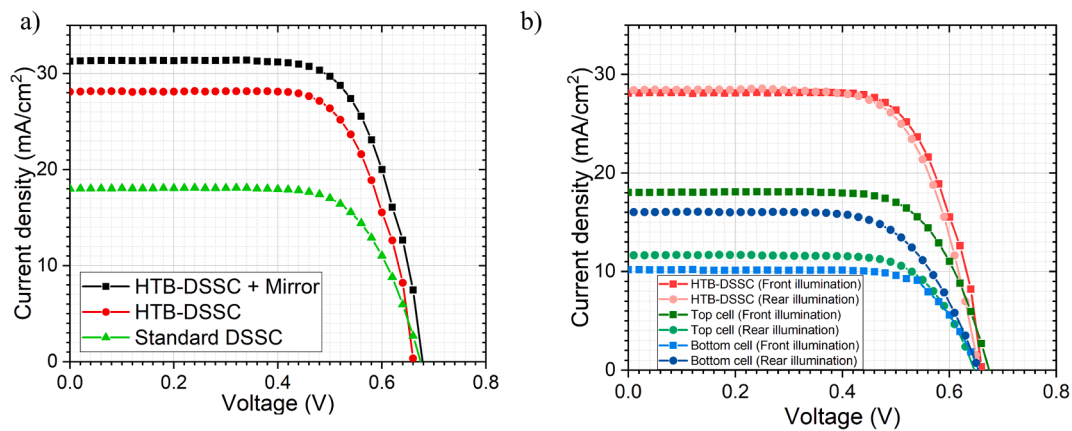
Fig. 2. J-V curves of the HTB-DSSC under AM 1.5G simulated solar spectrum in different configurations. (a) Comparison between standard solar cell and HTB-DSSC configuration, with and without back reflecting mirror. (b) Comparison between front and rear illumination and performances of top and bottom half-cells.

benefits from the increased photocurrent coming from the double absorbing layer, but with a higher open circuit voltage and a higher fill factor confirmed by the higher resistance to shunt losses, which can be reasonably connected to the lower thickness of the photoanodes.

Being the two half-cells of the HTB-DSSC configuration connected in parallel, the comparison with a planar module made by two standard DSSC connected in parallel was performed. The results of the characterization performed under AM 1.5G solar spectrum are reported in Fig. A2 and Table A2. As it can be seen from the current–voltage characteristic reported in Fig. A2.a, the planar module showed an absolute current, which was doubled with respect to a single standard solar cell and clearly higher with respect to the absolute current obtained by the HTB-DSSC configuration. On the other hand, looking at Fig. A2.b it can be observed how, normalizing the current with respect to the total active area of the different devices, the performance of the planar module resulted almost identical with respect to the one of the standard single DSSC. The HTB-DSSC, instead, benefited from the higher photogenerated current with respect to the standard solar cell, but obtained with the same total active area, confirming how the proposed configuration could be exploited to improve the performance of DSSCs without compromising on the total footprint of the device.

Together with the performance improvements granted by the stacked configuration, similar to what happens for tandem solar cells, the HTB-DSSC ensures also the possibility of collecting light incoming from both directions as the case of bifacial solar cells. It can be observed from Fig. 2b that, when the S-DSSC is illuminated in front and rear illumination, it yields a very similar behavior, showing PCE values of 13.19 and 12.8%, respectively, and a bifaciality factor as high as 0.97, which results to be much higher with respect to other bifacial DSSCs reported in the literature, for which, to the best of our knowledge, the best value was 0.78 under 1 sun illumination condition [33]. This remarkable result is intrinsically granted by the symmetrical nature of the proposed configuration, and it is expected to be further improvable if a more automated and controlled fabrication procedure is employed to prepare the two half-cells. As a matter of fact, as it can be seen in Fig. 2b and in Table A3, the top half-cell and the bottom half-cell show slightly different photovoltaic parameters when characterized under standard AM 1.5G simulated solar spectrum. The same difference is observed when the half-cells are characterized singularly in shielded condition, i. e., when they are illuminated through the other half-cell of the HTB-DSSC. Nevertheless, when they are connected in parallel, their performances compensate, yielding an almost equal PCE in front and rear illuminations. From this it can be stated that, as long as the disparity between the half-cells is kept at a minimum through a controlled and repeatable fabrication process, the HTB-DSSC is able to reach impressive levels of bifaciality.

One of the fields of application where DSSCs have demonstrated to outperform other photovoltaic technologies is the generation of photovoltaic energy under artificial (or even natural) illumination in indoor environments [8]. The absorption spectrum of most common sensitizing dyes employed in DSSCs is usually limited to visible light wavelengths. This is one of the main reasons of DSSCs lower performances with respect to other photovoltaic technologies when employed under standard AM1.5 solar spectrum, which includes a consistent amount of energy in the UV and IR region that cannot be collected by the cell. On the other hand, the most common indoor light sources, such as LED lights and fluorescent tubes, are typically optimized to emit in the visible spectrum only, and at much lower intensities with respect to external sunlight. The better spectral matching between DSSCs absorption and indoor lights emission ranges, together with the performance increase in DSSCs when they are employed in diffused and low-intensity illumination, motivates the rising interest in the scientific community toward the optimization of DSSCs under visible light [13,22,32]. Based on this, we characterized the HTB-DSSC also when illuminated with a commercial indoor low consuming LED light. A dedicated set-up was employed to simulate an indoor environment, based on the specifications reported by Sacco et al. [28]. A picture of the set-up is reported in Fig. A3 and it allows to simulate the effects of diffusing walls that usually become relevant in indoor environments. In Fig. 3a, the J-V curves of the HTB-DSSC under LED light illumination are reported. The illuminance value was 1200 lux, which corresponded to an incident power density of 0.38 mW cm^{-2}. The corresponding numerical values of the photovoltaic parameters are reported in Table 2.

As it can be seen, also under indoor light illumination the beneficial effect of the HTB-DSSC is observed, with an increased J_{sc} in HTB configuration with respect to the standard solar cell. Under 1200 lux illumination, the HTB-DSSC shows a J_{sc} of 184.88 µA cm^{-2} and a PCE of 19.94%, opposed to the 129.66 µA cm^{-2} and 14.52% generated by the standard solar cell, with a 37% relative increase in the conversion efficiency. Looking at Table 2, the effect of the HTB configuration on the V_{oc}, previously observed for standard AM 1.5G illumination, is present again and becomes more evident since the incident light intensity is much reduced under indoor light conditions with respect to simulated solar light. The same observations can be done looking at the J-V curves and at the corresponding photovoltaic parameters, measured at different light intensities under the LED indoor lamp, which are reported in Fig. A4 and Table A4, respectively. Apart from the already commented case at 1200 lux, the cells were tested at three more illumination levels, 1400 lux, 1800 lux and 2000 lux, which corresponded to incident power densities of 0.45 mW cm^{-2}, 0.59 mW cm^{-2} and 0.65 mW cm^{-2}, respectively. As expected, increasing the illuminance level, the J_{sc} of the HTB-DSSC rise proportionally, increasing from the value of 184.88 µA cm^{-2} measured at 1200 lux to 325.35 µA cm^{-2} at 2000 lux. The V_{oc} slightly increased from 0.55 V to 0.58 V and the fill factor remained
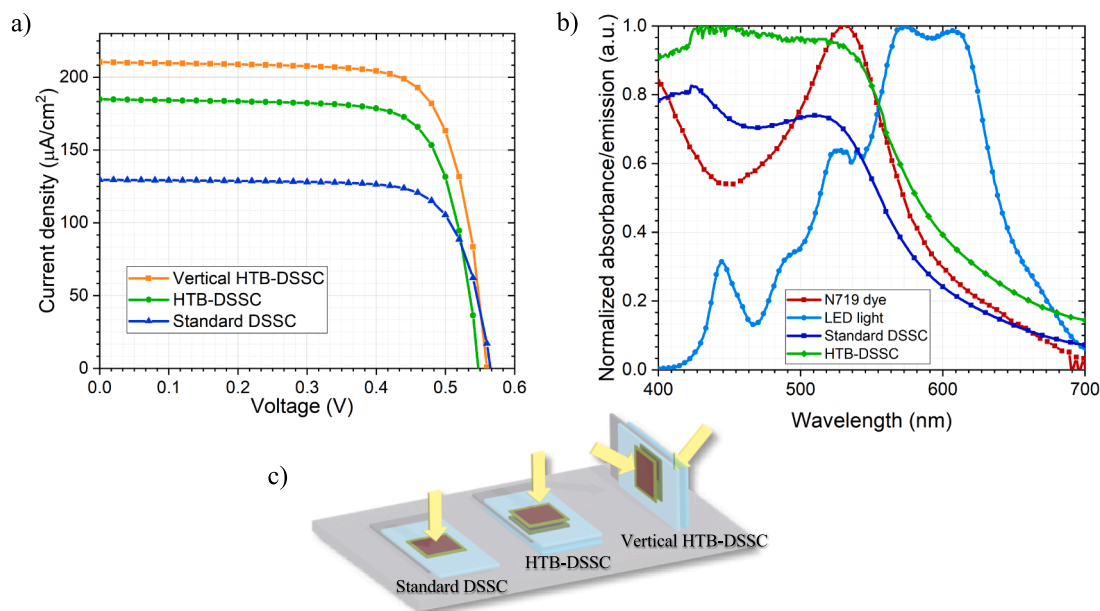
Fig. 3. a) J-V curves of the HTB-DSSC in flat and vertical configuration compared to the standard DSSC under 1200 lux indoor illumination. b) Comparison of the emission spectrum of the LED indoor light and the absorption spectrum of the N719 dye, the HTB-DSSC, and the standard DSSC. c) 3D representation of flat standard, HTB-DSSC and vertical HTB-DSSC configuration.

Table 2
Summarized photovoltaic parameters under LED indoor light illumination at 1200 lux (0.38 mW cm^{-2}).

Configuration	V_{oc} (V)	J_{sc} (μA cm^{-2})	FF	PCE (%)
Standard DSSC	0.57	129.66	0.76	14.52
HTB-DSSC	0.55	184.88	0.75	19.94
Vertical HTB-DSSC	0.56	210.42	0.75	23.18

almost unchanged, at high levels of 0.75. Consequently, the conversion efficiencies slightly increased from 19.9% at 1200 lux to 21.8% at 2000 lux with maximum power densities of 76.3 μW cm^{-2} and 143.4 μW cm^{-2}, respectively. The figures for the intermediate illuminance values of 1400 lux and 1800 lux stayed in between these values, as reported in Table A4. Overall, the HTB-DSSC configuration showed its potential also when employed under indoor illumination conditions. Moreover, it was suggested that the impressive bifaciality achieved by the HTB-DSSC could be used to further improve its performances under artificial illumination. As a matter of fact, often the presence, in indoor environments, of diffusing walls and objects becomes relevant in the spatial distribution of light. For this reason, the HTB-DSSC was characterized by keeping its top and bottom surfaces parallel to the vertical walls of the measurement set-up, in the so-called vertical configuration. The position of the solar cell inside the chamber was kept the same with respect to the measurements performed on the standard flat HTB-DSSC, and the incident power density for the efficiency calculation was the one measured in the same position with the photo-radiometer. This choice was made since, in a real indoor environment, the power output of an indoor solar cell would be estimated based on the measured incident power density in the desired position where the cell would be placed. A demonstration picture of the setup and of the vertical configuration is reported in Fig. A3. Being an unusual configuration, the measurements were made to give an idea of the potential that a HTB-DSSC could have, in the same environment, but placed vertical instead of flat. In this position, the HTB-DSSC is able not only to convert the light directly coming from the LED light source, but also the radiation which is re-diffused by the walls of the measurement set-up. The resulting J-V is reported in Fig. 3a, from which it can be observed that, under an illuminance of 1200 lux, the

current photogenerated by the cell increases, stepping from 184.88 μA cm^{-2} to 210.42 μA cm^{-2}, as a result of the higher amount of light that is converted by the HTB-DSSC. The open circuit voltage and the fill factor remains almost unchanged with the efficiency, calculated as previously described, that rise from 19.94% to 23.18%. Table A4 reports the photovoltaic parameters recorded at different illuminance levels, which show the same trend observed for standard flat measurements. The highest efficiency was recorded under 2000 lux where a value of 25.41% was obtained. These results suggest that a HTB-DSSC employed in vertical configuration could bring further advantages in application in indoor environments, where it could be used as a "light antenna", maximizing the conversion of light radiation diffused by walls and other objects. For example, portable devices such as monitoring sensors typical of the Internet of Things (IoT) sector could be realized integrating a small HTB-DSSC module placed in vertical configuration that could enable self-powering thanks to diffused ambient light.

Further insights on the effect of the HTB configuration on the light harvesting performances can be given comparing the absorbance of the HTB-DSSC and the standard cell in the visible part of the light spectrum, as reported in Fig. 3b. The absorption spectrum of the N719 dye and the emission spectrum of the LED light employed for indoor characterization are reported for comparison. It is clear how the HTB-DSSC shows a higher absorbance across the whole visible spectrum. This improvement becomes even more relevant for wavelengths between 550 and 700 nm, where the absorbance of the N719 dye starts to decrease. This is the region where the emission spectrum of the LED lamp has its maximum, therefore the increased absorbance shown by the HTB-DSSC with respect to the standard cell allows to further harness the energy emitted by the light source. It is clear that, by carefully engineering the sensitizing dyes, the absorption spectrum of the solar cell can be further optimized for use under indoor light and, if combined with the HTB-DSSC configuration, impressive levels of PCE can be achieved. This applies also to the emergent field of aqueous DSSCs, the latter featuring sustainability, safety and costs perfectly matching with technologies being in direct contact with humans [7,10].

3. Conclusions

In conclusion, it was demonstrated that the HTB-DSSC configuration

convincingly represents a simple and smart solution to enhance the photoconversion efficiency of DSSCs above the limit, regardless of the materials employed. Under standard AM 1.5G illumination condition, the HTB-DSSC fabricated with common N719 dye and I-based electrolyte shows a PCE of 13.19% under front illumination, which could be enhanced to 14.96% if a reflecting mirror is added on the back of the cell, generating a maximum output power of 13.19 and 14.96 mW cm^{-2}, respectively. Noteworthy, the HTB-DSSC also allows to be used in bifacial configuration, reaching a bifaciality factor as high as 0.97. It was observed that, to reach high levels of bifaciality taking full advantage of the HTB configuration, the difference between the two half-cells of the HTB-DSSC should be reduced to a minimum. Moreover, being the HTB-DSSC composed of two identical stacked half-cells connected in parallel, the dependence of the V_{oc} of the cell from the light intensity should be reduced as much as possible. Straightforwardly, when employed under indoor illumination, the HTB-DSSC reached impressive PCE values, ranging from 19.9 to 21.8% when the light illuminance was varied from 1200 to 2000 lux, with a 37% increase in photovoltaic performances with respect to the standard solar cell. It was shown that the HTB configuration could be used to take advantage of the presence of diffusing walls and other objects often found in indoor environments by employing the HTB-DSSC in vertical configuration, namely keeping the top and bottom faces of the solar cell perpendicular to the table surface. In this configuration, for illuminance from 1200 lux to 2000 lux, PCE values ranging from 23.2 to 25.4% were achieved. For future developments, it is suggested that the HTB-DSSC configuration could be coupled with the recent advancements on sensitizing dyes and alternative redox couples to easily reach outstanding levels of photovoltaic efficiency for dye-sensitized solar cells.

Author contributions

The manuscript was written through contributions of all authors. All authors have given approval to the final version of the manuscript.

Declaration of competing interest

The authors declare that they have no known competing financial interests or personal relationships that could have appeared to influence the work reported in this paper.

Acknowledgements

Appendix A. Supplementary data

Supplementary data to this article can be found online at https://doi.org/10.1016/j.solener.2023.112116.

References

[1] A. Agrawal, S.A. Siddiqui, A. Soni, G.D. Sharma, Advancements, frontiers and analysis of metal oxide semiconductor, dye, electrolyte and counter electrode of dye sensitized solar cell, Sol. Energy 233 (2022) 378–407, https://doi.org/10.1016/j.solener.2022.01.027.

[2] E.J. Beard, J.M. Cole, Perovskite- and dye-sensitized solar-cell device databases auto-generated using ChemDataExtractor, Sci. Data 9 (2022) 329, https://doi.org/10.1038/s41597-022-01355-w.

[3] T. Bhavani K, D.N. Joshi, V. Dutta, Tandem DSSC fabrication by controlled infiltration of organic dyes in mesoporous electrode using electric-field assisted spray technique, Sol. Energy 223 (2021) 318–325.

[4] G. Boschloo, E.A. Gibson, A. Hagfeldt, Photomodulated voltammetry of iodide/triiodide redox electrolytes and its relevance to dye-sensitized solar cells, J. Phys. Chem. Lett. 2 (2011) 3016–3020, https://doi.org/10.1021/jz2014314.

[5] G. Boschloo, A. Hagfeldt, Characteristics of the iodide/triiodide redox mediator in dye-sensitized solar cells, Acc. Chem. Res. 42 (2009) 1819–1826, https://doi.org/10.1021/ar900138m.

[6] D.A. Chalkias, C. Charalampopoulos, A.K. Andreopoulou, A. Karavioti, E. Stathatos, Spectral engineering of semi-transparent dye-sensitized solar cells using new triphenylamine-based dyes and an iodine-free electrolyte for greenhouse-oriented applications, J. Power Sources 496 (2021), 229842, https://doi.org/10.1016/j.jpowsour.2021.229842.

[7] J.C. de Haro, E. Tatsi, L. Fagiolari, M. Bonomo, C. Barolo, S. Turri, F. Bella, G. Griffini, Lignin-based polymer electrolyte membranes for sustainable aqueous dye-sensitized solar cells, ACS Sustain. Chem. Eng. 9 (2021) 8550–8560, https://doi.org/10.1021/acssuschemeng.1c01882.

[8] D. Devadiga, M. Selvakumar, P. Shetty, M.S. Santosh, Dye-sensitized solar cell for indoor applications: A mini-review, J. Electron. Mater. 50 (2021) 3187–3206, https://doi.org/10.1007/s11664-021-08854-3.

[9] M. Dhonde, K. Sahu, M. Das, A. Yadav, P. Ghosh, V.V.S. Murty, Review—Recent advancements in dye-sensitized solar cells; from photoelectrode to counter electrode, J. Electrochem. Soc. 169 (6) (2022), https://doi.org/10.1149/1945-7111/ac741f.

[10] S. Galliano, F. Bella, M. Bonomo, F. Giordano, M. Grätzel, G. Viscardi, A. Hagfeldt, C. Gerbaldi, C. Barolo, Xanthan-based hydrogel for stable and efficient quasi-solid truly aqueous dye-sensitized solar cell with cobalt mediator, Sol. RRL 5 (2021) 2000823, https://doi.org/10.1002/solr.202000823.

[11] Y. Gao, V.M. Le Corre, A. Gaïtis, M. Neophytou, M.A. Hamid, K. Takanabe, P.M. Beaujuge, Homo-tandem polymer solar cells with V_{OC} >1.8 V for efficient PV-driven water splitting, Adv. Mater. 28 (2016) 3366–3373, https://doi.org/10.1002/adma.201504633.

[12] B. Godefroid, G. Kozyreff, Photonic enhancement of parallel homo-tandem solar cells through the central electrode, Sol. Energy Mater. Sol. Cells 193 (2019) 73–79, https://doi.org/10.1016/j.solmat.2018.12.034.

[13] G. Gokul, S.C. Pradhan, S. Soman, Dye-sensitized solar cells as potential candidate for indoor/diffused light harvesting applications: From BIPV to self-powered IoTs, in: Tyagi, H., Agarwal, A.K., Chakraborty, P.R., Powar, S. (Eds.), Advances in Solar Energy Research, Energy, Environment, and Sustainability. Springer Singapore, Singapore, pp. 281–316. https://doi.org/10.1007/978-981-13-3302-6_9.

[14] M. Grätzel, Recent advances in sensitized mesoscopic solar cells, Acc. Chem. Res. 42 (2009) 1788–1798, https://doi.org/10.1021/ar900141y.

[15] M. Grätzel, Solar energy conversion by dye-sensitized photovoltaic cells, Inorg. Chem. 44 (2005) 6841–6851, https://doi.org/10.1021/ic0508371.

[16] F. Grifoni, M. Bonomo, W. Naim, N. Barbero, T. Alnasser, I. Dzeba, M. Giordano, A. Tsaturyan, M. Urbani, T. Torres, C. Barolo, F. Sauvage, Toward sustainable, colorless, and transparent photovoltaics: State of the art and perspectives for the development of selective near-infrared dye-sensitized solar cells, Adv. Energy Mater. 11 (2021) 2101598, https://doi.org/10.1002/aenm.202101598.

[17] N.T. Ho, H.N. Tien, S.-J. Jang, V. Senthilkumar, Y.C. Park, S. Cho, Y.S. Kim, Enhancement of recombination process using silver and graphene quantum dot embedded intermediate layer for efficient organic tandem cells, Sci. Rep. 6 (2016) 30327, https://doi.org/10.1038/srep30327.

[18] K. Kakiage, Y. Aoyama, T. Yano, K. Oya, J. Fujisawa, M. Hanaya, Highly-efficient dye-sensitized solar cells with collaborative sensitization by silyl-anchor and carboxy-anchor dyes, Chem. Commun. 51 (2015) 15894–15897, https://doi.org/10.1039/C5CC06759F.

[19] J.S. Kang, J. Kim, J.-Y. Kim, M.J. Lee, J. Kang, Y.J. Son, J. Jeong, S.H. Park, M.J. Ko, Y.-E. Sung, Highly efficient bifacial dye-sensitized solar cells employing polymeric counter electrodes, ACS Appl. Mater. Interfaces 10 (2018) 8611–8620, https://doi.org/10.1021/acsami.7b17815.

[20] R. Kang, S. Park, Y.K. Jung, D.C. Lim, M.J. Cha, J.H. Seo, S. Cho, High-efficiency polymer homo-tandem solar cells with carbon quantum-dot-doped tunnel junction intermediate layer, Adv. Energy Mater. 8 (2018) 1702165, https://doi.org/10.1002/aenm.201702165.

[21] M. Kokkonen, P. Talebi, J. Zhou, S. Asgari, S.A. Soomro, F. Elsehrawy, J. Halme, S. Ahmad, A. Hagfeldt, S.G. Hashmi, Advanced research trends in dye-sensitized solar cells, J. Mater. Chem. A 9 (2021) 10527–10545, https://doi.org/10.1039/D1TA00690H.

[22] H. Michaels, I. Benesperi, M. Freitag, Challenges and prospects of ambient hybrid solar cell applications, Chem. Sci. 12 (2021) 5002–5015, https://doi.org/10.1039/D0SC06477G.

[23] H. Michaels, M. Rinderle, R. Freitag, I. Benesperi, T. Edvinsson, R. Socher, A. Gagliardi, M. Freitag, Dye-sensitized solar cells under ambient light powering machine learning: towards autonomous smart sensors for the internet of things, Chem. Sci. 11 (2020) 2895–2906, https://doi.org/10.1039/C9SC06145B.

[24] M.K. Nazeeruddin, F. De Angelis, S. Fantacci, A. Selloni, G. Viscardi, P. Liska, S. Ito, B. Takeru, M. Grätzel, Combined experimental and DFT-TDDFT computational study of photoelectrochemical cell ruthenium sensitizers, J. Am. Chem. Soc. 127 (2005) 16835–16847, https://doi.org/10.1021/ja052467l.

[25] B. O'Regan, M. Grätzel, A low-cost, high-efficiency solar cell based on dye-sensitized colloidal TiO2 films, Nature 353 (1991) 737–740, https://doi.org/10.1038/353737a0.

[26] T.E. Putri, F.L. Chawarambwa, M.-K. Son, P. Attri, K. Kamataki, N. Itagaki, K. Koga, M. Shiratani, Performance characteristics of bifacial dye-sensitized solar cells with a V-shaped low-concentrating light system, ACS Appl. Energy Mater. 4 (2021) 13410–13414, https://doi.org/10.1021/acsaem.1c02774.

[27] D.F.S.L. Rodrigues, F. Santos, C.M.R. Abreu, J.F.J. Coelho, A.C. Serra, D. Ivanou, A. Mendes, Passivation of the TiO$_2$ surface and promotion of N719 dye anchoring with poly(4-vinylpyridine) for efficient and stable dye-sensitized solar cells, ACS Sustain. Chem. Eng. 9 (2021) 5981–5990, https://doi.org/10.1021/acssuschemeng.1c00842.

[28] A. Sacco, L. Rolle, L. Scaltrito, E. Tresso, C.F. Pirri, Characterization of photovoltaic modules for low-power indoor application, Appl. Energy 102 (2013) 1295–1302, https://doi.org/10.1016/j.apenergy.2012.07.001.

[29] A. Sacco, R. Speranza, U. Savino, J. Zeng, M.A. Farkhondehfal, A. Lamberti, A. Chiodoni, C.F. Pirri, An integrated device for the solar-driven electrochemical conversion of CO$_2$ to CO, ACS Sustain. Chem. Eng. 8 (2020) 7563–7568, https://doi.org/10.1021/acssuschemeng.0c02088.

[30] S. Sasidharan, S.C. Pradhan, A. Jagadeesh, B.N. Nair, A.A.P. Mohamed, N.U. K. n, S. Soman, U.N.S. Hareesh, Bifacial dye-sensitized solar cells with enhanced light scattering and improved power conversion efficiency under full sun and indoor light conditions, ACS Appl. Energy Mater. 3 (12) (2020) 12584–12595, https://doi.org/10.1021/acsaem.0c02500.

[31] H.J. Snaith, L. Schmidt-Mende, M. Grätzel, M. Chiesa, Light intensity, temperature, and thickness dependence of the open-circuit voltage in solid-state dye-sensitized solar cells, Phys. Rev. B 74 (2006), 045306, https://doi.org/10.1103/PhysRevB.74.045306.

[32] R. Speranza, P. Zaccagnini, A. Sacco, A. Lamberti, High-voltage energy harvesting and storage system for internet of things indoor application, Sol. RRL (2022), 2200245, https://doi.org/10.1002/solr.202200245.

[33] S. Venkatesan, Y. Cho, I.-P. Liu, H. Teng, Y. Lee, Novel architecture of indoor bifacial dye-sensitized solar cells with efficiencies surpassing 25% and efficiency ratios exceeding 95%, Adv. Opt. Mater. 9 (2021), 2100936 https://doi.org/10.1002/adom.202100936.

[34] S. Venkatesan, T.-H. Hsu, X.-W. Wong, H. Teng, Y.-L. Lee, Tandem dye-sensitized solar cells with efficiencies surpassing 33% under dim-light conditions, Chem. Eng. J. 446 (2022), 137349, https://doi.org/10.1016/j.cej.2022.137349.

[35] S. Venkatesan, W.-H. Lin, H. Teng, Y.-L. Lee, High-efficiency bifacial dye-sensitized solar cells for application under indoor light conditions, ACS Appl. Mater. Interfaces 11 (2019) 42780–42789, https://doi.org/10.1021/acsami.9b14876.

[36] Z.-S. Wang, H. Kawauchi, T. Kashima, H. Arakawa, Significant influence of TiO2 photoelectrode morphology on the energy conversion efficiency of N719 dye-sensitized solar cell, Coord. Chem. Rev. 248 (2004) 1381–1389, https://doi.org/10.1016/j.ccr.2004.03.006.

[37] T. Yamaguchi, Y. Uchida, S. Agatsuma, H. Arakawa, Series-connected tandem dye-sensitized solar cell for improving efficiency to more than 10%, Sol. Energy Mater. Sol. Cells 93 (2009) 733–736, https://doi.org/10.1016/j.solmat.2008.09.021.

[38] L. Yuan, H. Michaels, R. Roy, M. Johansson, V. Öberg, A. Andruszkiewicz, X. Zhang, M. Freitag, E.M.J. Johansson, Four-terminal tandem solar cell with dye-sensitized and PbS colloidal quantum-dot-based subcells, ACS Appl. Energy Mater. 3 (2020) 3157–3161, https://doi.org/10.1021/acsaem.0c00030.